catalysts

MDPI

Article

Photocatalytic Degradation of 4-tert-butylphenol Using Solar Light Responsive Ag_2CO_3

Saule Mergenbayeva [1], Timur Sh. Atabaev [2], John Vakros [3,4], Dionissios Mantzavinos [3] and Stavros G. Poulopoulos [1,*]

[1] Department of Chemical and Materials Engineering, School of Engineering and Digital Sciences, Nazarbayev University, Astana 010000, Kazakhstan
[2] Department of Chemistry, School of Sciences and Humanities, Nazarbayev University, Astana 010000, Kazakhstan
[3] Department of Chemical Engineering, University of Patras, Caratheodory 1, University Campus, GR-26504 Patras, Greece
[4] School of Sciences and Engineering, University of Nicosia, Nicosia 2417, Cyprus
* Correspondence: stavros.poulopoulos@nu.edu.kz; Tel.: +7-7172-694608

Abstract: In this work, Ag_2CO_3 was prepared via a solution-based method and was further characterized by XRD, Raman spectroscopy, SEM/EDS analysis, and UV-VIS spectroscopy. SEM results revealed the formation of micro-sized particles with a rectangular shape. The photocatalytic activity of the catalyst was evaluated in the degradation of 4-tert-butylphenol (4-t-BP) under simulated solar light irradiation. The effects of 4-t-BP initial concentration (2.5–10 ppm), catalyst dosage (100–300 mg/L), different types of lamp sources, and water matrix were investigated. Complete 4-t-BP (5 ppm) degradation was achieved after 60 min by Ag_2CO_3 (200 mg/L). The effect of anions such as CO_3^{2-}, HCO_3^-, NO_3^-, and Cl^- in the concentration range of 100–300 mg/L was also studied. CO_3^{2-} promoted the photocatalytic degradation process, while HCO_3^- and NO_3^- exhibited an inhibition effect, which was marked with increasing HCO_3^- and NO_3^- concentrations. The presence of Cl^- at the concentration of 100 mg/L increased 4-t-BP degradation, but higher concentrations inhibited the photocatalytic reaction. Cyclic experiments showed that the catalyst practically retained its catalytic activity toward 4-t-BP degradation after three successive experimental runs.

Keywords: 4-tert-butylphenol; degradation; heterogeneous photocatalysis; solar light

check for updates

Citation: Mergenbayeva, S.; Atabaev, T.S.; Vakros, J.; Mantzavinos, D.; Poulopoulos, S.G. Photocatalytic Degradation of 4-tert-butylphenol Using Solar Light Responsive Ag_2CO_3. *Catalysts* **2022**, *12*, 1523. https://doi.org/10.3390/catal12121523

Academic Editors: Krzysztof Miecznikowski and Beata Krasnodębska-Ostręga

Received: 26 October 2022
Accepted: 23 November 2022
Published: 26 November 2022

1. Introduction

4-tert-butylphenol (4-t-BP) is an important organic chemical that is extensively used as an intermediate in the production of curing agents [1], phenolic, polycarbonate, and epoxy resins, etc., but is also an endocrine disrupting compound (EDC) [2]. Recently, 4-t-BP has been detected in water bodies from ng/L to µg/L, representing an environmental threat to aquatic life and human health [3–8]. Therefore, it is of great importance to seek an effective process to degrade 4-t-BP in water.

Several treatment technologies such as photochemical [9–11], physical [12], and biological [13] techniques have been investigated for the efficient elimination of 4-t-BP in contaminated water. Among these, advanced oxidation processes (AOPs) are considered promising to achieve a high degree of 4-t-BP degradation in an environmentally friendly manner [14,15]. Table 1 lists several works regarding AOPs previously used to degrade 4-t-BP. Particularly, heterogeneous photocatalysis, based on the activation of a solid semiconductor with solar light [16–18], has received increasing attention and is considered as an economically and environmentally viable method, since it applies an inexhaustible and sustainable energy source. The sunlight provides abundant irradiation energy; most of it is in the visible light range and only ~4% is ultraviolet light [19,20]. Thus, it is highly desirable to develop a solar-light responsive catalyst.

Table 1. Application of different AOPs for 4-t-BP degradation in recent years.

	Processes	Initial Pollutant Concentration (mg/L)	Catalyst Dosage (g/L)	Degradation Time (min)	Degradation Efficiency (%)	Reference
1	Visible light/$Bi_4O_5I_2$ nanoflakes	60	1	90	99.8	[11]
2	Visible light/$Bi_{12}O_{17}Cl_2$/β-Bi_2O_3 heterojunction (Bi:Cl ratio 1:8)	60	1	90	97	[21]
3	UV(254 nm)/Fe-TiO_2	30	1	60	92	[22]
4	Solar light/Ti_2O_3/TiO_2	5	0.2	150	89.8	[23]
5	UV (365 nm)/Cu-Mo-TiO_2	15	0.1	60	100	[24]

To date, many new solar light active catalysts have emerged to degrade EDCs in water, such as metal and bimetal doped metal oxides [24], and binary and ternary composites [25–30]. Ag-based semiconductor materials like Ag_2O [31,32], AgX (where X = Cl, Br, I) [33], etc. have spawned great interest in photocatalysis because of their non-toxicity [34] and useful photo-absorption ability, particularly in the visible light spectrum [35]. Among the Ag-based photocatalytic materials, Ag_2CO_3 has a relatively narrow band gap of 2.3 eV [36], while the bottom of its conduction band (CB) consists of hybridized Ag s-Ag s states responsible for high dispersity, which in turn effectively hinders the recombination of electrons and holes [37]. Several researchers have previously reported the photocatalytic activity of Ag_2CO_3 prepared via different methods. Dai et al. used highly visible-light responsive micro-sized Ag_2CO_3 for the degradation of rhodamine B (RhB) [36]. Porous Ag_2CO_3 nanorods prepared using a one-pot aqueous solution method were also applied for the degradation of RhB under visible light irradiation by Guo et al. [38]. In 2017, Lončarević et al. [39] and Zhou et al. [40] reported the photodegradation of methylene blue by means of Ag_2CO_3 nano-rods and nanoparticles. Recently, Petala et al. found that Ag_2CO_3 could completely degrade ethyl paraben with possible carcinogenic activity at the concentration of 0.5 mg/L after 120 min under solar light irradiation [37]. However, most of these studies focused on the degradation of organic dyes, while the photocatalytic activity of Ag_2CO_3 toward the degradation of high estrogenic organic compounds is still under-researched. To the best of our knowledge, there is no study published on the photocatalytic degradation of 4-t-BP, which is a toxic and estrogenic compound, using Ag_2CO_3.

In this study, Ag_2CO_3 microparticles were prepared and employed for 4-t-BP degradation under solar light irradiation. The crystal phase and morphology were investigated using X-ray diffraction analysis (XRD), Raman spectroscopy and Scanning electron microscopy (SEM). The influence of pollutant concentration, catalyst dosage, various light sources and the presence of anions (Cl^-, HCO_3^- and CO_3^{2-}) was investigated. Radical trapping experiments were performed to study the mechanism of the photocatalytic degradation of 4-t-BP in Ag_2CO_3/solar light system.

2. Results and Discussion

2.1. Characterization

The phase purity and crystallographic structure of Ag_2CO_3 was investigated through XRD analysis as displayed in Figure 1. The results reveal that Ag_2CO_3 was in the monoclinic phase without impurities, corresponding to the JCPDS card No. 12-766 [37]. The characteristic diffraction peaks at 18.55°, 20.5°, 32.56°, 33.64°, 37.04°, 39.56°, 41.73°, and 44.32° were attributed to the (020), (110), (−101), (−130), (200), (031), (220), and (131) planes, which is in accordance with the standard XRD pattern of Ag_2CO_3 [41,42]. Raman spectroscopy was applied in order to support the structural information obtained via XRD analysis. As shown in Figure 2, two peaks at around 701 cm^{-1} and 1073 cm^{-1} were observed, which corresponded to the characteristic Raman spectra of Ag_2CO_3 [43,44].

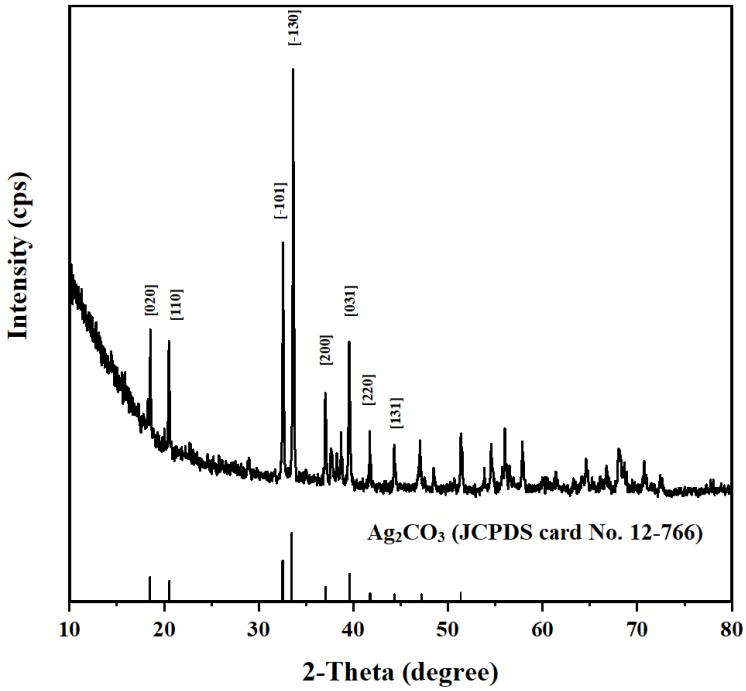

Figure 1. XRD pattern of Ag_2CO_3.

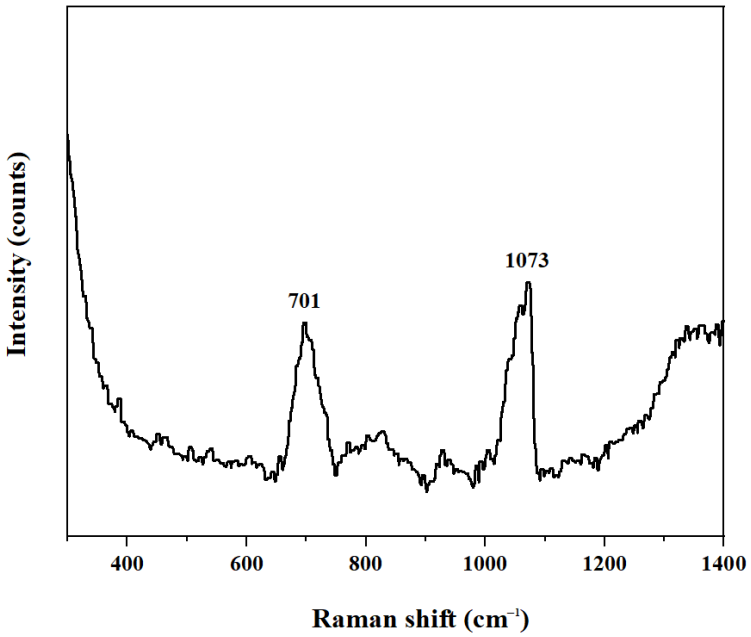

Figure 2. Raman spectrum of Ag_2CO_3.

In order to study the morphology of Ag_2CO_3, SEM analysis was conducted. The SEM image (Figure 3A) revealed that Ag_2CO_3 particles are micro-sized with a smooth rectangular structure. The EDS spectrum of Ag_2CO_3 (Figure 3B) showed that Ag, C, and O had an elemental distribution of 73.13 wt%, 6.74 wt%, and 20.13 wt%, respectively. At the same time, the elemental mapping showed a homogeneous distribution of Ag, C, and O elements (Figure 3C–F), confirming the purity of the Ag_2CO_3 phase. These findings are in agreement with XRD and Raman measurements.

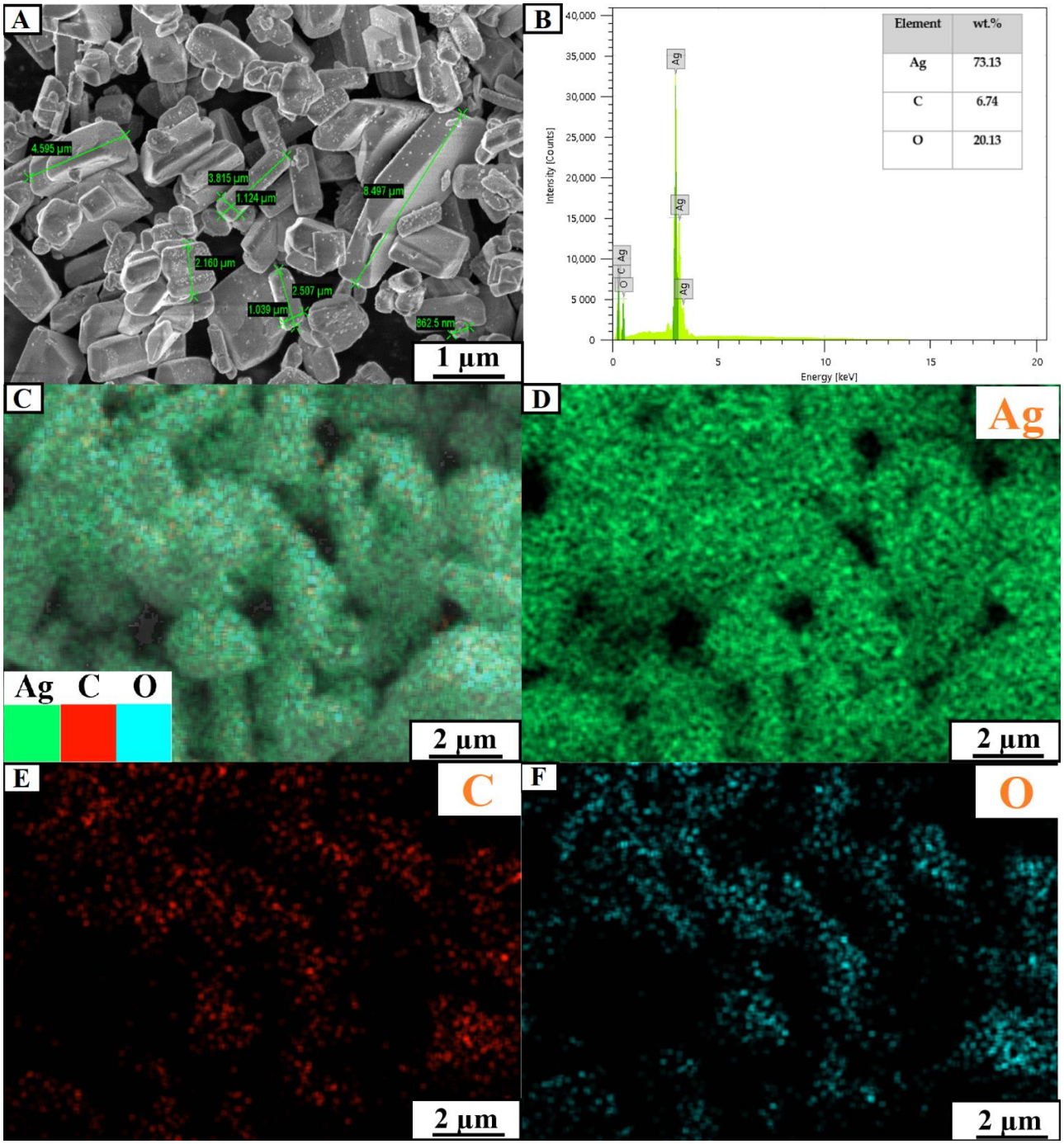

Figure 3. (**A**) SEM image, (**B**) EDS spectrum, and (**C**–**F**) Elemental mapping of Ag_2CO_3.

The optical absorption properties of Ag_2CO_3 were examined using UV-VIS spectroscopy. Figure 4 shows that the catalyst had sufficient absorbance of light below 350 nm, and in the ranges of 350–450 nm and 450–800 nm, suggesting that Ag_2CO_3 could be photocatalytically active under both UV and visible light as a result of the intrinsic absorption band of Ag_2CO_3 [45]. The band gap estimated through Tauc plot of Ag_2CO_3 was found to be 2.3 eV. These findings are in agreement with previous studies [46,47].

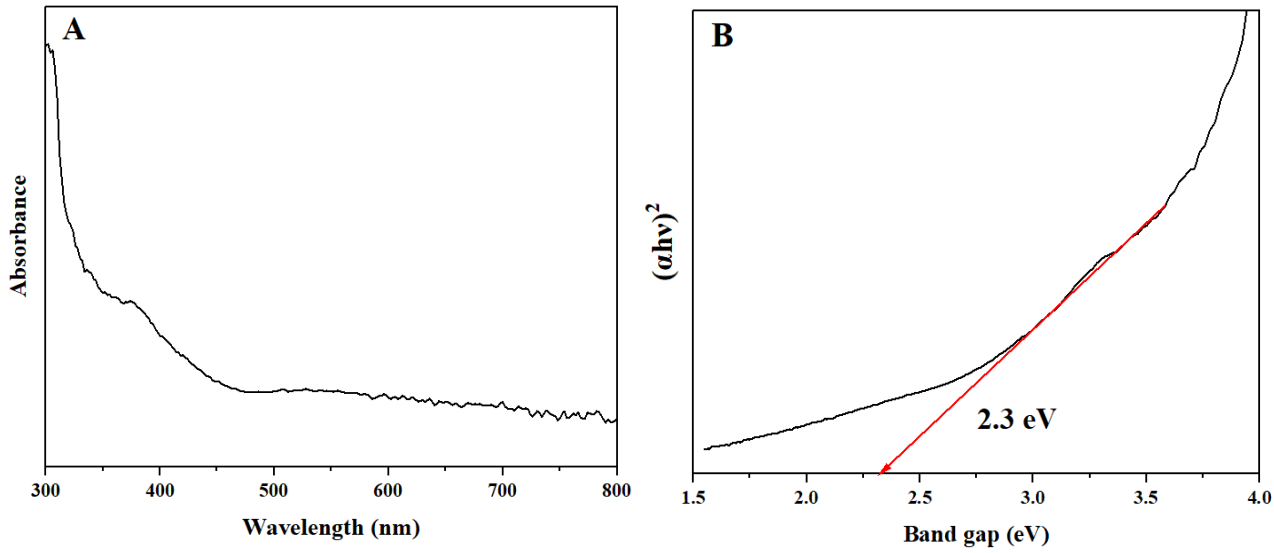

Figure 4. (**A**) UV-VIS spectra and (**B**) Tauc plot of Ag_2CO_3.

2.2. *Photocatalytic Activity of Ag_2CO_3*

2.2.1. Effect of 4-t-BP Initial Concentration and Catalyst Dosage

4-t-BP was used as the target degradation compound to examine the solar photocatalytic activity of Ag_2CO_3. Figure 5A shows the effect of initial 4-t-BP concentration on 4-t-BP degradation. The degradation efficiency increased with the increase in pollutant initial concentration from 2.5 ppm to 5 ppm, while it was remarkably decreased after 60 min, with a further increase of pollutant initial concentration to 7.5 and 10 ppm. Such an observation implies a negative correlation between pollutant concentration and degradation efficiency, and can be associated with the fact that more molecules of 4-t-BP would compete to occupy limited reactive sites on the catalyst surface [48–50].

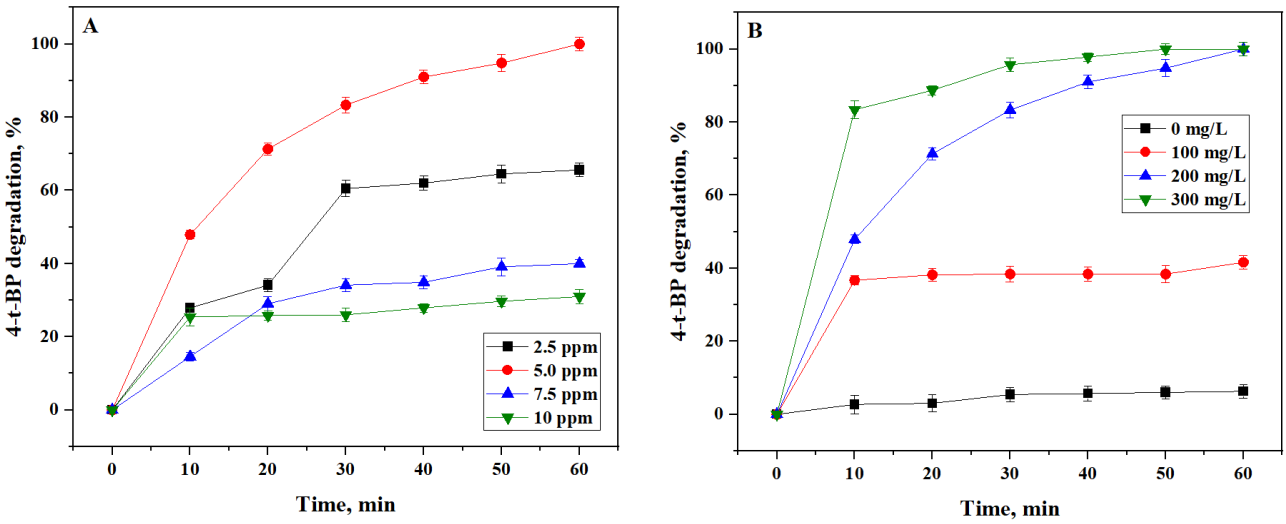

Figure 5. (**A**) Effect of initial 4-t-BP concentration (catalyst dosage = 200 mg/L) and (**B**) Effect of catalyst dosage ($[4\text{-t-BP}]_0$ = 5 ppm) on the degradation of 4-t-BP under solar light.

To study the effect of Ag_2CO_3 on the degradation of 4-t-BP, different Ag_2CO_3 dosages (100, 200, and 300 mg /L) were used. As shown in Figure 5B, only 6.3% of 4-t-BP was degraded after 60 min in the absence of catalyst, indicating that 4-t-BP could not be effectively degraded by solar light only. As expected, 4-t-BP degradation was enhanced when the catalyst was added to the solution. The increase in catalyst dosage from 100 mg/L to 300 mg/L led to the increase of the final degradation efficiency from 41.6% to 100%. This

can be attributed to the existence of a higher amount of active sites, leading to significant increase in the 4-t-BP degradation [51–53]. On the other hand, the degradation performance of the catalyst was almost the same at the dosages of 200 mg/L and 300 mg/L after 60 min. This could be explained by the reduction of light penetration because of the agglomeration of catalyst microparticles [54,55]. Therefore, the dosage of 200 mg/L was used in the next experimental runs.

The results obtained in this work are compared to selected previous works on the use of Ag_2CO_3-based catalysts in the photodegradation of organic pollutants, in Table 2. Most of the recent studies focused on the preparation of composites, including ternary and quaternary, and their application under visible/solar light irradiation. Depending on the pollutant, its initial concentration, catalyst dosage, and light source, the degradation efficiency varies.

Table 2. The recent application of Ag_2CO_3-based catalysts for the degradation of organic compounds in water, under light irradiation.

	Catalyst	Pollutant	Light Source	Degradation Time (min)	Degradation Efficiency (%)	Reference
1	$CaMg(CO_3)_2$@Ag_2CO_3/Ag_2S/NCQD	phenol	Simulated solar	100	96.5	[56]
2	Ag_2O/Ag_2CO_3/MWNTs	ciprofloxacin	visible light	60	76	[41]
3	In_2O_3/Ag_2CO_3 S-scheme heterojunction	levofloxacin	visible light	90	86.1	[57]
4	Ag_2CO_3@Fe_2O_3/TiO_2-NT	phenol	solar	240	96.2	[58]
5	g-C_3N_4/Ag_2CO_3/graphene oxide	tetracycline	visible	60	81.6	[59]
6	ZnO/Ag_2CO_3/Ag_2O	ibuprofen	visible	480	99.3	[60]
7	Ag_2CO_3 microparticles	4-tert-butylphenol	Simulated solar	60	100	this work

2.2.2. Effect of Lamp Type

Photocatalytic degradation of 4-t-BP by Ag_2CO_3 using a Mercury lamp (365 nm, 500 W) and a Xenon lamp (Xe, 300–600 nm, 500 W) was also conducted to compare results with the solar light simulating Xenon lamp (100 W). As displayed in Figure 6, after 10 min, the degradation efficiency of Ag_2CO_3 using the Xe lamp (300–600 nm) was higher than for the solar light simulating lamp and Mercury lamp (365 nm), achieving 63.6% of 4-t-BP degradation. The application of the Xe lamp (300–600 nm) led to an almost similar degradation efficiency as that of the Mercury lamp (365 nm), though complete degradation of 4-t-BP was achieved only under the solar light simulating Xenon lamp (solar) after 60 min. Such behavior could be associated with the wide range of light absorption of Ag_2CO_3, showing concordance with the UV-VIS spectroscopy results of this study.

The energy cost of the photocatalytic process for the degradation of organic pollutants is one of the most important aspects influencing the implementation of these technologies at a larger scale. The energy consumption can be identified through the electrical energy per order (EE_o), and calculated according to the Equation (1):

$$EE_o = \frac{P \times t \times 1000}{V \times 60 \times \log\left(\frac{C_i}{C_f}\right)} \quad (1)$$

where P is the power of the lamp (W); t is the photocatalytic reaction time (min); V is the volume of the reactor (L); and C_i and C_f are the initial and final concentrations of 4-t-BP, respectively.

The calculated EE_o value (Table 3) for the degradation of 4-t-BP, applying the Xe lamp (solar) is 0.98 kWh m^{-3} $order^{-1}$, which is significantly lower than the Hg lamp (365 nm) and Xe lamp (300–600 nm), for which values 8–9 times higher are estimated.

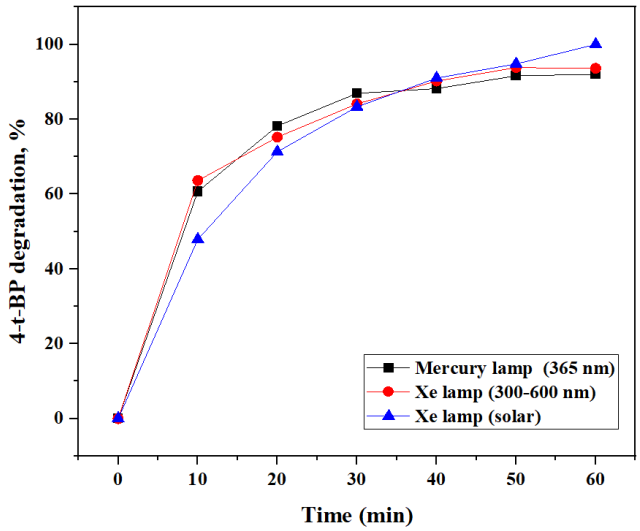

Figure 6. Effect of lamp types on the degradation of 4-t-BP. Experimental conditions: $[4\text{-t-BP}]_0$ = 5 ppm, catalyst dosage = 200 mg/L.

Table 3. EE_O estimated for different type of lamps.

Light Source	EE_O (kW m^{-3} $order^{-1}$)
Hg lamp (365 nm)	9.12
Xe lamp (300–600 nm)	8.29
Xe lamp (solar light)	0.98

2.2.3. Effect of Water Matrix

Natural water matrices consist of a great number of organic and inorganic substances that can interfere with the target pollutant, either promoting or suppressing the efficiency of the process [61,62]. Bottled water is a typical representative of water matrices and therefore the photocatalytic efficiency of the Ag_2CO_3/solar system was also studied in commercially available bottled water (BW). The properties of BW are presented in Table 4. As can be seen from Figure 7, the degradation of 4-t-BP decreased during the first 40 min for BW, which could be attributed to the water matrix complexity [61]. Therefore, additional experiments were conducted to thoroughly investigate the hampering role of BW by adding anions like CO_3^{2-}, HCO_3^-, NO_3^-, and Cl^- in the range of of 100–300 mg/L.

Table 4. The properties of bottled water.

Properties	Value
Conductivity	158.8 µS/cm
pH	7.2
Total organic carbon (TOC)	1.02 mg/L
Total inorganic carbon	16.72 mg/L
Na^+	1–15 mg/L
K^+	0–5 mg/L
Ca^{2+}	10–45 mg/L
Mg^{2+}	5–25 mg/L
HCO_3^-	50–200 mg/L
Cl^-	3–35 mg/L
SO_4^{2-}	1–30 mg/L

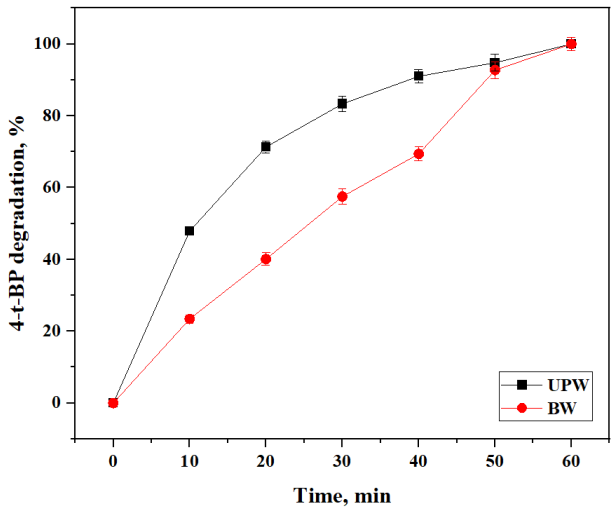

Figure 7. Effect of the type of water on the degradation of 4-t-BP under solar light. Experimental conditions: $[4\text{-t-BP}]_0$ = 5 ppm, catalyst dosage = 200 mg/L.

As shown in Figure 8A, the presence of CO_3^{2-} enhanced the 4-t-BP degradation. Increasing the concentration of CO_3^{2-} from 100 mg/L to 300 mg/L led to the improvement of catalyst performance. Such behavior could be attributed to the generation of more active species ($CO_3^{\bullet-}$) in the reaction system (Equation (2)). Although $CO_3^{\bullet-}$ has a lower redox potential than that of $OH^{\bullet}$, it exhibits higher selectivity and longer survival time in solution, resulting in fast 4-t-BP photocatalytic degradation in the reaction system [63,64].

$$OH^{\bullet} + CO_3^{2-} \rightarrow CO_3^{\bullet-} + OH^- \quad (2)$$

As for HCO_3^- and NO_3^- (Figure 8B,C), the significant inhibition effect on the performance of Ag_2CO_3 stems from the formation of less reactive radicals [65,66] (Equation (3)) and the consumption of photons, $OH^{\bullet}$ and h^+ by NO_3^- [67] (Equations (4)–(6)). The most pronounced inhibition effect of $HCO_3^{\bullet}$ and $NO_3^{\bullet}$ was observed with an increase of HCO_3^- and NO_3^- concentrations to 300 mg/L. The degradation efficiency of 4-t-BP decreased to 55.1% and 50.6% in the presence of HCO_3^- and NO_3^-, respectively.

$$HCO_3^- + OH^{\bullet} \rightarrow CO_3^{\bullet-} + H_2O \quad (3)$$

$$NO_3^- + h\nu \rightarrow NO_2^- O \quad (4)$$

$$NO_2^- + OH^{\bullet} \rightarrow OH^- + NO_2 \quad (5)$$

$$NO_3^- + h^+ \rightarrow NO_3^{\bullet} \quad (6)$$

The addition of 100 mg/L of Cl^- had a positive effect on the degradation process ascribed to the selectivity of chloride radicals [68], while a further increase in Cl^- concentration inhibited the photocatalytic degradation of 4-t-BP (Figure 8D). This can be associated with the generation of less oxidative species via the following reactions [69,70] (Equations (7)–(14)):

$$Cl^- + OH^{\bullet} \rightarrow Cl^{\bullet} + OH^- \quad (7)$$

$$Cl^- + OH^{\bullet} \rightarrow ClOH^{\bullet-} \quad (8)$$

$$ClOH^{\bullet-} + H^+ \rightarrow Cl^{\bullet} + H_2O \quad (9)$$

$$Cl^{\bullet} + Cl^- \rightarrow Cl_2^{\bullet-} \quad (10)$$

$$Cl_2^{\bullet-} + Cl_2^{\bullet-} \rightarrow Cl_2 + 2Cl^- \quad (11)$$

$$Cl^{\bullet} + Cl^{\bullet} \rightarrow Cl_2 \quad (12)$$

$$Cl_2 + H_2O \rightarrow HOCl + HCl \quad (13)$$

$$HOCl \rightarrow H^+ + ClO^- \quad (14)$$

To investigate the photocatalytic mechanism of Ag_2CO_3, radical quenching experiments were performed using several scavengers, namely KI, IPA, and p-BQ to identify the major active species (h^+, $OH^\bullet$, and $O_2^{\bullet-}$) responsible for the degradation of 4-t-BP. The degradation efficiency was enhanced in all three cases (Figure 9), suggesting that the presence of KI, IPA, and p-BQ was beneficial for the Ag_2CO_3/solar light system in terms of 4-t-BP degradation. The introduction of KI into the reaction contributed to the production of more $OH^\bullet$ radicals through the scavenging of photo-generated h^+ [63,71], while the addition of IPA decreased the recombination of electron-holes [72], hence increasing the photocatalytic activity.

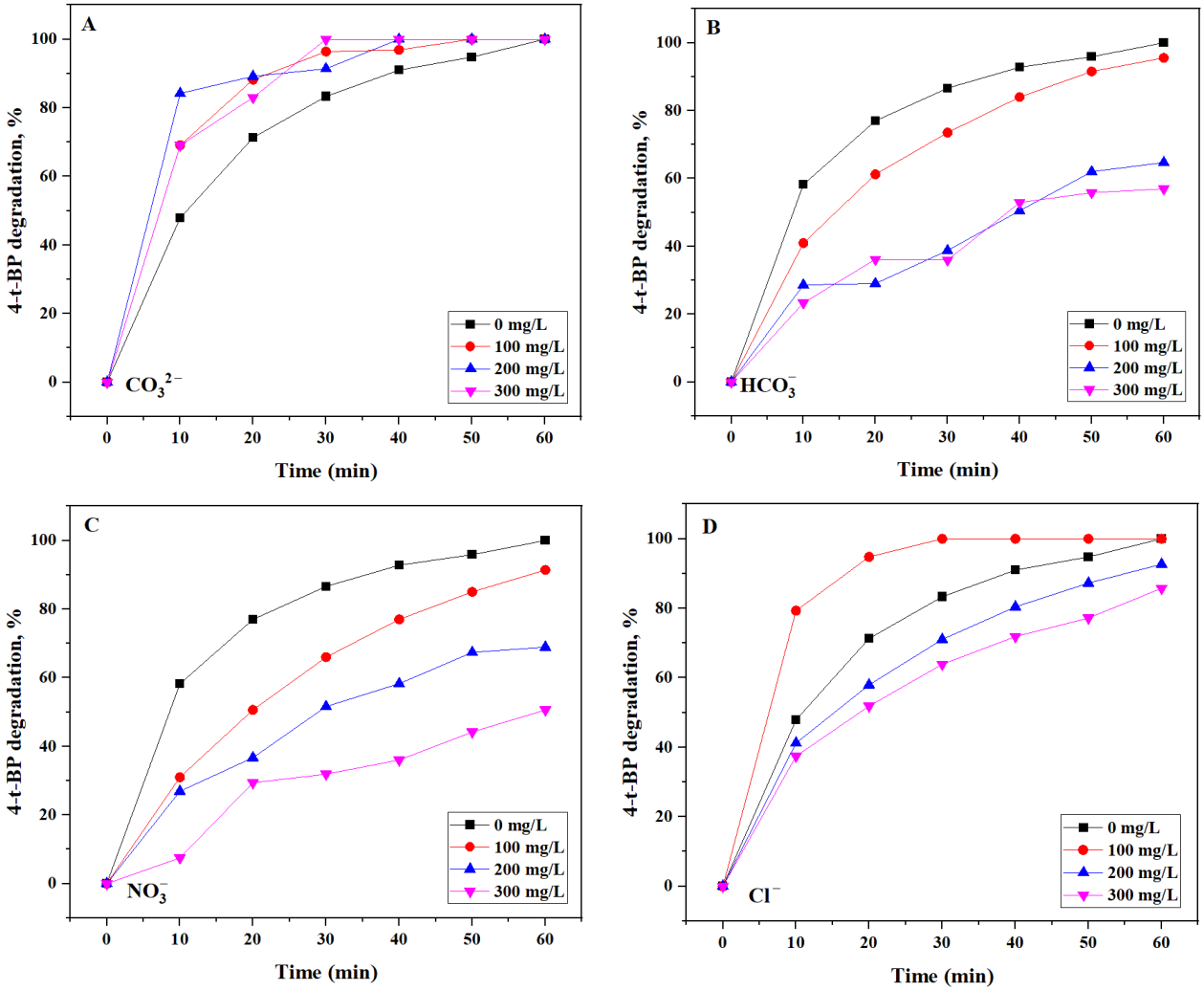

Figure 8. The effect of (**A**) CO_3^{2-}, (**B**) HCO_3^-, (**C**) NO_3^-, and (**D**) Cl^- on the degradation of 4-t-BP. Experimental conditions: $[4\text{-t-BP}]_0$ = 5 ppm, catalyst dosage = 200 mg/L.

As previously reported [36], the visible light irradiation of Ag_2CO_3 catalyst results in the formation of electrons/holes in Ag_2CO_3 (Equation (15)), resulting in electron transfer. Positive holes react with water generating $OH^\bullet$ (Equation (16)), while electrons may induce both oxidation (Equation (17)) and reduction reactions (Equation (18)) leading to the formation of H_2O_2 and CO_3^{2-} radicals.

$$Ag_2CO_3 + h\nu \rightarrow Ag_2CO_3\,(h^+ + e^-) \quad (15)$$

$$H_2O + h^+ \rightarrow OH^{\bullet} + H^+ \quad (16)$$

$$O_2 + 2H^+ + 2e^- \rightarrow H_2O_2 \quad (17)$$

$$Ag_2CO_3 + 2e^- \rightarrow 2Ag + CO_3^{2-} \quad (18)$$

It has also been reported that in some cases, radical scavenging tests had no remarkable impact on the degradation of persistent organic pollutant, suggesting the presence of surface-bound reactive species and electron transfer in the reaction solution between the oxidant and the molecule of the target organic compound [63]. In such cases, H_2O_2 formed under the absorption of visible light by Ag_2CO_3 (Equation (17)) can serve as an oxidant in the degradation process, while the generated CO_3^{2-} radical (Equation (18)) promotes the degradation of 4-t-BP, as discussed earlier.

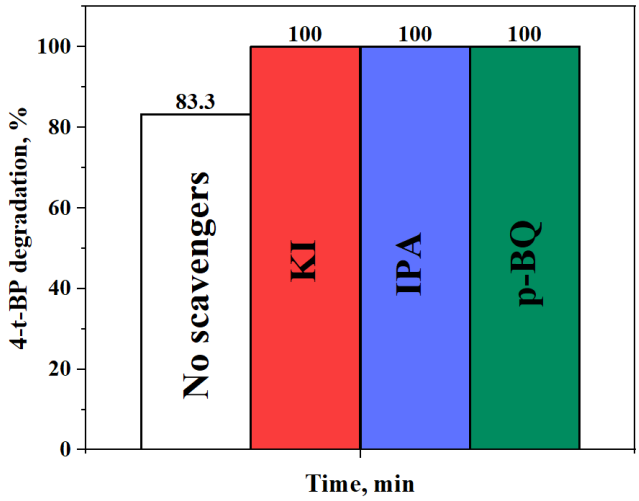

Figure 9. Effect of KI, IPA, and p-BQ on the degradation of 4-t-BP. Experimental conditions: $[4\text{-t-BP}]_0$ = 5 ppm, catalyst dosage = 200 mg/L.

2.2.4. Reusability and Stability of Ag_2CO_3

Cyclic experiments were carried out to investigate the stability and reusability of the Ag_2CO_3 catalyst. Figure 10 illustrates the performance of the Ag_2CO_3 catalyst for three successive experiments. After each run, the catalyst was filtered, washed with UPW for several times, and dried. It is obvious that the loss in catalytic activity of Ag_2CO_3 was insignificant, thus indicating the good stability of the catalyst.

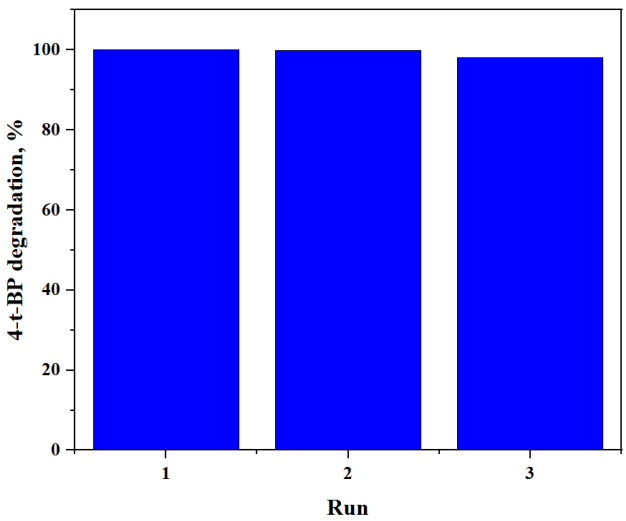

Figure 10. Cyclic experiments of Ag_2CO_3 toward the degradation of 4-t-BP. Experimental conditions: $[4\text{-t-BP}]_0$ = 5 ppm, catalyst dosage = 200 mg/L.

3. Materials and Methods

3.1. Materials

Silver nitrate ($AgNO_3$, 99.0%), 4-tert-butylphenol (HO-C_6H_4-C-$(CH_3)_3$, 99.0%), sodium carbonate (Na_2CO_3, 99.5%), sodium bicarbonate ($NaHCO_3$, 99.7%), sodium nitrate ($NaNO_3$, 99.0%), sodium chloride (NaCl, 99.8%), methanol (CH_3OH, 99.9%) were obtained from Sigma-Aldrich (Saint Louis, MO, USA), while potassium iodide (KI, 99.0%), isopropanol (C_3H_8O, 99.5%) p-benzoquinone ($C_6H_4O_2$, 98.0%) were obtained from Merck KGaA (Darmstadt, Germany) and used without further purification. UPW (18.25 MΩ*cm) was applied for preparing required solutions.

3.2. Preparation of Ag_2CO_3

A simple solution-based method was used to synthesize Ag_2CO_3 [73]. Under continuous stirring, two solutions were prepared: (1) 0.5 g of $NaHCO_3$ was mixed in 60 mL of UPW and (2) 2.04 g of $AgNO_3$ was mixed in 60 mL UPW. Then, the obtained $AgNO_3$ mixture was added dropwise to $NaHCO_3$ mixture and kept under a stirring condition for 240 min at room temperature. Finally, the formed precipitate was collected by centrifugation, washed with UPW, and dried at 60 °C for 12 h.

3.3. Characterization of the Prepared Catalyst

The XRD pattern of prepared Ag_2CO_3 was recorded on the Rigaku Smartlab system (Rigaku, Tokyo, Japan) in a 2θ range of 10–80°, while the Raman spectra was obtained using Raman spectrometer (Horiba, LabRam HR evolution, Kyoto, Japan). SEM imaging and EDS elemental mapping of Ag_2CO_3 analysis was performed using a SEM/EDS (Crossbeam 540, Carl Zeiss, Oberkochen, Germany) instrument. UV-VIS spectroscopy was used to investigate the optical properties of the catalyst by Thermo Scientific Genesys 150 UV–Visible spectrophotometer (Thermo Fisher Scientific Inc., Waltham, MA, USA).

3.4. Photocatalytic Degradation of 4-t-BP

Photocatalytic experiments were conducted in a 50 mL batch reactor under continuous stirring. A solar simulator (100 W Xe lamp, AM1.5G filter, LCS-100, Newport) was used as an irradiation source. The initial concentration of 4-t-BP ranged from 2.5–10 ppm (mg/L), while the catalyst dosage amounted in the range of 0–300 mg/L. A 30-min magnetic stirring was applied before the start of irradiation to allow for adsorption-desorption equilibrium. Samples were periodically withdrawn from the reactor, filtered by means of 0.22 µm Millipore filters, and sent for high-performance liquid chromatography (HPLC, Agilent 1290 Infinity II, Santa Clara, CA, USA) analysis. A mixture of CH_3OH and UPW (50%:50% by volume) was used as a mobile phase.

The following equation was used to estimate the 4-t-BP degradation:

$$\text{Degradation } (\%) = \frac{C_0 - C_t}{C_t} \times 100\%$$

where C_t is the concentration of 4-t-BP after regular intervals of time (t), and C_0 is the initial concentration of 4-t-BP.

For comparison, the 4-t-BP solution in the presence of Ag_2CO_3 was also exposed using a Mercury lamp (365 nm, 500 W) and a Xenon lamp (300–600 nm, 500 W) source under the same conditions using photocatalytic reactors (Lanphan industry, Zhengzhou City, Henan Province, China).

The active species in the Ag_2CO_3/solar light system were investigated with the addition of potassium iodide (KI), isopropanol (IPA), and p-benzoquinone (p-BQ) into the reaction system to identify holes (h^+), hydroxyl radicals ($OH^\bullet$), and superoxide radicals ($O_2^{\bullet-}$), respectively. Prior to irradiation, 1 mL of each scavenger solution, with a concentration of 2 mmol/L was added to the mixture of 4-t-BP solution and Ag_2CO_3.

4. Conclusions

Ag_2CO_3 was synthesized by a simple solution-based method and was applied toward 4-t-BP degradation under simulated solar light irradiation. The crystal structure, purity, morphology, and optical properties of the catalyst were studied using XRD, Raman Spectroscopy, SEM, and UV-VIS spectroscopy. The effect of different factors, including the initial concentration of 4-t-BP, catalyst dosage, types of light source, and water matrix on 4-t-BP degradation were further investigated. Complete degradation of 4-t-BP (5 ppm) was achieved within 60 min using 200 mg/L of Ag_2CO_3. The presence of CO_3^{2-} had only a positive effect on the performance of Ag_2CO_3/solar light system and enhanced 4-t-BP degradation. Low amounts of Cl^- (100 mg/L) in the reaction system enhanced 4-t-BP degradation; however, a further increase of Cl^- concentration to 300 mg/L inhibited the degradation process. Through three successive experimental runs, the catalyst exhibited excellent stability and reusability properties.

Author Contributions: Conceptualization, S.G.P. and D.M.; methodology, J.V. and S.G.P.; investigation, S.M. and J.V.; resources, S.G.P., T.S.A. and D.M.; writing—original draft preparation, S.M.; writing—review and editing, S.G.P., T.S.A., J.V. and D.M.; supervision, T.S.A. and S.G.P.; project administration, S.G.P. All authors have read and agreed to the published version of the manuscript.

Funding: This research was funded by the Nazarbayev University project "Cost-Effective Photocatalysts for the Treatment of Wastewaters containing Emerging Pollutants", Faculty Development Competitive Research Grants Program for 2020–2022, Grant Number 240919FD3932, awarded to S.G. Poulopoulos.

Data Availability Statement: Not applicable.

Acknowledgments: The technical support of the Core Facilities of Nazarbayev University is greatly acknowledged.

Conflicts of Interest: The authors declare no conflict of interest.

References

1. Bell, A.M.; Baier, R.; Kocher, B.; Reifferscheid, G.; Buchinger, S.; Ternes, T. Ecotoxicological Characterization of Emissions from Steel Coatings in Contact with Water. *Water Res.* **2020**, *173*, 115525. [CrossRef] [PubMed]
2. Toyama, T.; Momotani, N.; Ogata, Y.; Miyamori, Y.; Inoue, D.; Sei, K.; Mori, K.; Kikuchi, S.; Ike, M. Isolation and Characterization of 4-Tert-Butylphenol-Utilizing Sphingobium Fuliginis Strains from Phragmites Australis Rhizosphere Sediment. *Appl. Environ. Microbiol.* **2010**, *76*, 6733–6740. [CrossRef]
3. Gao, X.; Huang, P.; Huang, Q.; Rao, K.; Lu, Z.; Xu, Y.; Gabrielsen, G.W.; Hallanger, I.; Ma, M.; Wang, Z. Organophosphorus Flame Retardants and Persistent, Bioaccumulative, and Toxic Contaminants in Arctic Seawaters: On-Board Passive Sampling Coupled with Target and Non-Target Analysis. *Environ. Pollut.* **2019**, *253*, 1–10. [CrossRef] [PubMed]
4. Liu, D.; Liu, J.; Guo, M.; Xu, H.; Zhang, S.; Shi, L.; Yao, C. Occurrence, Distribution, and Risk Assessment of Alkylphenols, Bisphenol A, and Tetrabromobisphenol A in Surface Water, Suspended Particulate Matter, and Sediment in Taihu Lake and Its Tributaries. *Mar. Pollut. Bull.* **2016**, *112*, 142–150. [CrossRef] [PubMed]
5. Liu, Y.-H.; Zhang, S.-H.; Ji, G.-X.; Wu, S.-M.; Guo, R.-X.; Cheng, J.; Yan, Z.-Y.; Chen, J.-Q. Occurrence, Distribution and Risk Assessment of Suspected Endocrine-Disrupting Chemicals in Surface Water and Suspended Particulate Matter of Yangtze River (Nanjing Section). *Ecotoxicol. Environ. Saf.* **2017**, *135*, 90–97. [CrossRef]
6. Xie, W.; Zhao, J.; Zhang, Q.; Ye, C.; Zheng, G.; Shan, Q.; Li, L.; Shao, X. Occurrence, Distribution and Bioaccumulation of Alkylphenols in the Pearl River Networks, South China. *Ecol. Indic.* **2020**, *110*, 105847. [CrossRef]
7. Kojima, M.; Tsunoi, S.; Tanaka, M. Determination of 4-Alkylphenols by Novel Derivatization and Gas Chromatography–Mass Spectrometry. *J. Chromatogr. A* **2003**, *984*, 237–243. [CrossRef]
8. Colin, A.; Bach, C.; Rosin, C.; Munoz, J.; Dauchy, X. Is Drinking Water a Major Route of Human Exposure to Alkylphenol and Bisphenol Contaminants in France? *Arch. Environ. Contam. Toxicol.* **2013**, *66*, 86–99. [CrossRef]
9. Wu, Y.; Brigante, M.; Dong, W.; de Sainte-Claire, P.; Mailhot, G. Toward a Better Understanding of Fe(III)–EDDS Photochemistry: Theoretical Stability Calculation and Experimental Investigation of 4-Tert-Butylphenol Degradation. *J. Phys. Chem. A* **2014**, *118*, 396–403. [CrossRef]
10. Mergenbayeva, S.; Poulopoulos, S.G. Comparative Study on UV-AOPs for Efficient Continuous Flow Removal of 4-Tert-Butylphenol. *Processes* **2022**, *10*, 8. [CrossRef]

11. Xiao, X.; Xing, C.; He, G.; Zuo, X.; Nan, J.; Wang, L. Solvothermal Synthesis of Novel Hierarchical $Bi_4O_5I_2$ Nanoflakes with Highly Visible Light Photocatalytic Performance for the Degradation of 4-Tert-Butylphenol. *Appl. Catal. B Environ.* **2014**, *148–149*, 154–163. [CrossRef]
12. del Rio, M.; Grimalt Escarabajal, J.C.; Turnes Palomino, G.; Palomino Cabello, C. Zinc/Iron Mixed-Metal MOF-74 Derived Magnetic Carbon Nanorods for the Enhanced Removal of Organic Pollutants from Water. *Chem. Eng. J.* **2022**, *428*, 131147. [CrossRef]
13. Ogata, Y.; Toyama, T.; Yu, N.; Wang, X.; Sei, K.; Ike, M. Occurrence of 4-Tert-Butylphenol (4-t-BP) Biodegradation in an Aquatic Sample Caused by the Presence of Spirodela Polyrrhiza and Isolation of a 4-t-BP-Utilizing Bacterium. *Biodegradation* **2013**, *24*, 191–202. [CrossRef] [PubMed]
14. Kanafin, Y.; Makhatova, A.; Arkhangelsky, E.; Poulopoulos, S. Photochemical Treatment of an Actual Municipal Wastewater by Means of UV, Potassium Persulfate and Iron. *IOP Conf. Ser. Earth Environ. Sci.* **2021**, *899*, 012067. [CrossRef]
15. Mergenbayeva, S.; Ashir, A.; Yergali, B.; Ulykbanova, G.; Poulopoulos, S. Modified TiO_2 for Photocatalytic Removal of Organic Pollutants in Water: 2nd International Conference on Environmental Design, ICED 2021. *IOP Conf. Ser. Earth Environ. Sci.* **2021**, *899*, 012068. [CrossRef]
16. Padovan, R.N.; de Carvalho, L.S.; de Souza Bergo, P.L.; Xavier, C.; Leitão, A.; dos Santos Neto, Á.J.; Lanças, F.M.; Azevedo, E.B. Degradation of Hormones in Tap Water by Heterogeneous Solar TiO_2-Photocatalysis: Optimization, Degradation Products Identification, and Estrogenic Activity Removal. *J. Environ. Chem. Eng.* **2021**, *9*, 106442. [CrossRef]
17. Taheri, M.E.; Petala, A.; Frontistis, Z.; Mantzavinos, D.; Kondarides, D.I. Fast Photocatalytic Degradation of Bisphenol A by Ag_3PO_4/TiO_2 Composites under Solar Radiation. *Catal. Today* **2017**, *280*, 99–107. [CrossRef]
18. Silva, T.F.C.V.; Peri, P.; Fajardo, A.S.; Paulista, L.O.; Soares, P.A.; Martínez-Huitle, C.A.; Vilar, V.J.P. Solar-Driven Heterogeneous Photocatalysis Using a Static Mixer as TiO_2-P25 Support: Impact of Reflector Optics and Material. *Chem. Eng. J.* **2022**, *435*, 134831. [CrossRef]
19. Zhang, W.; He, H.; Li, H.; Duan, L.; Zu, L.; Zhai, Y.; Li, W.; Wang, L.; Fu, H.; Zhao, D. Visible-Light Responsive TiO_2-Based Materials for Efficient Solar Energy Utilization. *Adv. Energy Mater.* **2021**, *11*, 2003303. [CrossRef]
20. Mohapatra, L.; Parida, K. A Review of Solar and Visible Light Active Oxo-Bridged Materials for Energy and Environment. *Catal. Sci. Technol.* **2017**, *7*, 2153–2164. [CrossRef]
21. He, G.; Xing, C.; Xiao, X.; Hu, R.; Zuo, X.; Nan, J. Facile Synthesis of Flower-like $Bi_{12}O_{17}Cl_2/\beta$-Bi_2O_3 Composites with Enhanced Visible Light Photocatalytic Performance for the Degradation of 4-Tert-Butylphenol. *Appl. Catal. B Environ.* **2015**, *170–171*, 1–9. [CrossRef]
22. Makhatova, A.; Ulykbanova, G.; Sadyk, S.; Sarsenbay, K.; Atabaev, T.S.; Inglezakis, V.J.; Poulopoulos, S.G. Degradation and Mineralization of 4-Tert-Butylphenol in Water Using Fe-Doped TiO_2 Catalysts. *Sci. Rep.* **2019**, *9*, 19284. [CrossRef] [PubMed]
23. Mergenbayeva, S.; Atabaev, T.S.; Poulopoulos, S.G. Ti_2O_3/TiO_2-Assisted Solar Photocatalytic Degradation of 4-Tert-Butylphenol in Water. *Catalysts* **2021**, *11*, 1379. [CrossRef]
24. Mergenbayeva, S.; Kumarov, A.; Atabaev, T.S.; Hapeshi, E.; Vakros, J.; Mantzavinos, D.; Poulopoulos, S.G. Degradation of 4-Tert-Butylphenol in Water Using Mono-Doped (M1: Mo, W) and Co-Doped (M2-M1: Cu, Co, Zn) Titania Catalysts. *Nanomaterials* **2022**, *12*, 2326. [CrossRef] [PubMed]
25. Monteagudo, J.M.; Durán, A.; Chatzisymeon, E.; San Martín, I.; Naranjo, S. Solar Activation of TiO_2 Intensified with Graphene for Degradation of Bisphenol-A in Water. *Solar Energy* **2018**, *174*, 1035–1043. [CrossRef]
26. Garg, A.; Singhania, T.; Singh, A.; Sharma, S.; Rani, S.; Neogy, A.; Yadav, S.R.; Sangal, V.K.; Garg, N. Photocatalytic Degradation of Bisphenol-A Using N, Co Codoped TiO_2 Catalyst under Solar Light. *Sci. Rep.* **2019**, *9*, 765. [CrossRef]
27. de la Flor, M.P.; Camarillo, R.; Martínez, F.; Jiménez, C.; Quiles, R.; Rincón, J. Synthesis and Characterization of Bimetallic TiO_2/CNT/Pd-Cu for Efficient Remediation of Endocrine Disruptors under Solar Light. *J. Environ. Chem. Eng.* **2022**, *10*, 107245. [CrossRef]
28. Singla, S.; Sharma, S.; Basu, S. MoS_2/WO_3 Heterojunction with the Intensified Photocatalytic Performance for Decomposition of Organic Pollutants under the Broad Array of Solar Light. *J. Clean. Prod.* **2021**, *324*, 129290. [CrossRef]
29. Zhang, Y.; Yu, H.; Li, S.; Wang, L.; Huang, F.; Guan, R.; Li, J.; Jiao, Y.; Sun, J. Rapidly Degradation of Di-(2-Ethylhexyl) Phthalate by Z-Scheme Bi_2O_3/TiO_2@reduced Graphene Oxide Driven by Simulated Solar Radiation. *Chemosphere* **2021**, *272*, 129631. [CrossRef]
30. Zhang, Y.; Shan, G.; Dong, F.; Wang, C.; Zhu, L. Glass Fiber Supported BiOI Thin-Film Fixed-Bed Photocatalytic Reactor for Water Decontamination under Solar Light Irradiation. *J. Environ. Sci.* **2019**, *80*, 277–286. [CrossRef]
31. Deekshitha; Shetty, V.K. Solar Light Active Biogenic Titanium Dioxide Embedded Silver Oxide ($AgO/Ag_2O@TiO_2$) Nanocomposite Structures for Dye Degradation by Photocatalysis. *Mater. Sci. Semicond. Process.* **2021**, *132*, 105923. [CrossRef]
32. Ran, R.; McEvoy, J.G.; Zhang, Z. Ag2O/Ag3VO4/Ag4V2O7 Heterogeneous Photocatalyst Prepared by a Facile Hydrothermal Synthesis with Enhanced Photocatalytic Performance under Visible Light Irradiation. *Mater. Res. Bull.* **2016**, *74*, 140–150. [CrossRef]
33. Zhao, Z.; Wang, Y.; Xu, J.; Shang, C.; Wang, Y. AgCl-Loaded Mesoporous Anatase TiO_2 with Large Specific Surface Area for Enhancing Photocatalysis. *Appl. Surf. Sci.* **2015**, *351*, 416–424. [CrossRef]
34. Du, J.; Ma, S.; Zhang, N.; Liu, W.; Lv, M.; Ni, T.; An, Z.; Li, K.; Bai, Y. Efficient Photocatalytic Organic Degradation and Disinfection Performance for $Ag/AgFeO_2/g$-C_3N_4 Nanocomposites under Visible-Light: Insights into the Photocatalysis Mechanism. *Colloids Surf. A Physicochem. Eng. Asp.* **2022**, *654*, 130094. [CrossRef]

35. Xu, B.; Li, Y.; Gao, Y.; Liu, S.; Lv, D.; Zhao, S.; Gao, H.; Yang, G.; Li, N.; Ge, L. Ag-AgI/Bi_3O_4Cl for Efficient Visible Light Photocatalytic Degradation of Methyl Orange: The Surface Plasmon Resonance Effect of Ag and Mechanism Insight. *Appl. Catal. B Environ.* **2019**, *246*, 140–148. [CrossRef]
36. Dai, G.; Yu, J.; Liu, G. A New Approach for Photocorrosion Inhibition of Ag2CO3 Photocatalyst with Highly Visible-Light-Responsive Reactivity. *J. Phys. Chem. C* **2012**, *116*, 15519–15524. [CrossRef]
37. Petala, A.; Nasiou, A.; Mantzavinos, D.; Frontistis, Z. Photocatalytic Evaluation of Ag_2CO_3 for Ethylparaben Degradation in Different Water Matrices. *Water* **2020**, *12*, 1180. [CrossRef]
38. Guo, S.; Bao, J.; Hu, T.; Zhang, L.; Yang, L.; Peng, J.; Jiang, C. Controllable Synthesis Porous Ag_2CO_3 Nanorods for Efficient Photocatalysis. *Nanoscale Res. Lett.* **2015**, *10*, 193. [CrossRef] [PubMed]
39. Lončarević, D.; Vukoje, I.; Dostanić, J.; Bjelajac, A.; Đorđević, V.; Dimitrijević, S.; Nedeljković, J.M. Antimicrobial and Photocatalytic Abilities of Ag_2CO_3 Nano-Rods. *ChemistrySelect* **2017**, *2*, 2931–2938. [CrossRef]
40. Zhou, L.; Liang, L.; Talifu, D.; Abulizi, A. Sonochemical Fabrication of Ag_2CO_3 Nanomaterial and Influencing Factors on Photocatalytic Properties. *IOP Conf. Ser. Mater. Sci. Eng.* **2017**, *167*, 012032. [CrossRef]
41. Wang, H.; Li, J.; Huo, P.; Yan, Y.; Guan, Q. Preparation of Ag_2O/Ag_2CO_3/MWNTs Composite Photocatalysts for Enhancement of Ciprofloxacin Degradation. *Appl. Surf. Sci.* **2016**, *366*, 1–8. [CrossRef]
42. Yu, C.; Wei, L.; Chen, J.; Xie, Y.; Zhou, W.; Fan, Q. Enhancing the Photocatalytic Performance of Commercial TiO_2 Crystals by Coupling with Trace Narrow-Band-Gap Ag_2CO_3. *Ind. Eng. Chem. Res.* **2014**, *53*, 5759–5766. [CrossRef]
43. Si, M.; Wang, W.; Guan, Q.; Zhang, H.; Puttaswamy, M. Facile Fabrication of Highly Catalytic-Active Ag_2CO_3/AgBr/Graphene Oxide Ternary Composites towards the Photocatalytic Wastewater Treatment. *Environ. Sci. Pollut. Res.* **2021**, *28*, 4173–4183. [CrossRef] [PubMed]
44. Wang, W.; Liu, Y.; Zhang, H.; Qian, Y.; Guo, Z. Re-Investigation on Reduced Graphene Oxide/Ag_2CO_3 Composite Photocatalyst: An Insight into the Double-Edged Sword Role of RGO. *Appl. Surf. Sci.* **2017**, *396*, 102–109. [CrossRef]
45. Li, T.; Hu, X.; Liu, C.; Tang, C.; Wang, X.; Luo, S. Efficient Photocatalytic Degradation of Organic Dyes and Reaction Mechanism with Ag2CO3/Bi2O2CO3 Photocatalyst under Visible Light Irradiation. *J. Mol. Catal. A Chem.* **2016**, *425*, 124–135. [CrossRef]
46. Xu, H.; Zhu, J.; Song, Y.; Zhu, T.; Zhao, W.; Song, Y.; Da, Z.; Liu, C.; Li, H. Fabrication of AgX-Loaded Ag_2CO_3 (X=Cl, I) Composites and Their Efficient Visible-Light-Driven Photocatalytic Activity. *J. Alloy. Compd.* **2015**, *622*, 347–357. [CrossRef]
47. Xu, H.; Zhu, J.; Song, Y.; Zhao, W.; Xu, Y.; Song, Y.; Ji, H.; Li, H. Ion-Exchange Preparation for Visible-Light-Driven Photocatalyst AgBr/Ag_2CO_3 and Its Photocatalytic Activity. *RSC Adv.* **2014**, *4*, 9139–9147. [CrossRef]
48. Lei, X.; You, M.; Pan, F.; Liu, M.; Yang, P.; Xia, D.; Li, Q.; Wang, Y.; Fu, J. $CuFe_2O_4$@GO Nanocomposite as an Effective and Recoverable Catalyst of Peroxymonosulfate Activation for Degradation of Aqueous Dye Pollutants. *Chin. Chem. Lett.* **2019**, *30*, 2216–2220. [CrossRef]
49. Ani, I.J.; Akpan, U.G.; Olutoye, M.A.; Hameed, B.H. Photocatalytic Degradation of Pollutants in Petroleum Refinery Wastewater by TiO_2- and ZnO-Based Photocatalysts: Recent Development. *J. Clean. Prod.* **2018**, *205*, 930–954. [CrossRef]
50. Jiang, L.; Yuan, X.; Zeng, G.; Liang, J.; Wu, Z.; Yu, H.; Mo, D.; Wang, H.; Xiao, Z.; Zhou, C. Nitrogen Self-Doped g-C_3N_4 Nanosheets with Tunable Band Structures for Enhanced Photocatalytic Tetracycline Degradation. *J. Colloid Interface Sci.* **2019**, *536*, 17–29. [CrossRef] [PubMed]
51. Wei, Y.; Zhang, Y.; Geng, W.; Su, H.; Long, M. Efficient Bifunctional Piezocatalysis of Au/$BiVO_4$ for Simultaneous Removal of 4-Chlorophenol and Cr(VI) in Water. *Appl. Catal. B Environ.* **2019**, *259*, 118084. [CrossRef]
52. Chen, F.; Yang, Q.; Li, X.; Zeng, G.; Wang, D.; Niu, C.; Zhao, J.; An, H.; Xie, T.; Deng, Y. Hierarchical Assembly of Graphene-Bridged Ag_3PO_4/Ag/$BiVO_4$ (040) Z-Scheme Photocatalyst: An Efficient, Sustainable and Heterogeneous Catalyst with Enhanced Visible-Light Photoactivity towards Tetracycline Degradation under Visible Light Irradiation. *Appl. Catal. B Environ.* **2017**, *200*, 330–342. [CrossRef]
53. Wang, Y.; Yu, L.; Wang, R.; Wang, Y.; Zhang, X. Microwave Catalytic Activities of Supported Perovskite Catalysts MOx/LaCo0.5Cu0.5O3@CM (M = Mg, Al) for Salicylic Acid Degradation. *J. Colloid Interface Sci.* **2020**, *564*, 392–405. [CrossRef] [PubMed]
54. Zeng, X.; Sun, X.; Yu, Y.; Wang, H.; Wang, Y. Photocatalytic Degradation of Flumequine with B/N Codoped TiO_2 Catalyst: Kinetics, Main Active Species, Intermediates and Pathways. *Chem. Eng. J.* **2019**, *378*, 122226. [CrossRef]
55. Al-Musawi, T.J.; Rajiv, P.; Mengelizadeh, N.; Mohammed, I.A.; Balarak, D. Development of Sonophotocatalytic Process for Degradation of Acid Orange 7 Dye by Using Titanium Dioxide Nanoparticles/Graphene Oxide Nanocomposite as a Catalyst. *J. Environ. Manag.* **2021**, *292*, 112777. [CrossRef] [PubMed]
56. Tian, J.; Liu, Z.; Zeng, D.; Yu, C.; Liu, X.; Yang, K.; Liu, H. The Preparation and Characterization of $CaMg(CO_3)_2$@Ag_2CO_3/Ag_2S/NCQD Nanocomposites and Their Photocatalytic Performance in Phenol Degradation. *J Nanopart Res* **2018**, *20*, 182. [CrossRef]
57. Shen, J.; Qian, L.; Huang, J.; Guo, Y.; Zhang, Z. Enhanced Degradation toward Levofloxacin under Visible Light with S-Scheme Heterojunction In_2O_3/Ag_2CO_3: Internal Electric Field, DFT Calculation and Degradation Mechanism. *Sep. Purif. Technol.* **2021**, *275*, 119239. [CrossRef]
58. El-Maghrabi, H.H.; Al-Kahlawy, A.A.; Nada, A.A.; Zaki, T. Photocorrosion Resistant Ag_2CO_3@Fe_2O_3/TiO_2-NT Nanocomposite for Efficient Visible Light Photocatalytic Degradation Activities. *J. Hazard. Mater.* **2018**, *360*, 250–256. [CrossRef] [PubMed]

59. Liu, H.-Y.; Liang, C.; Niu, C.-G.; Huang, D.-W.; Du, Y.-B.; Guo, H.; Zhang, L.; Yang, Y.-Y.; Zeng, G.-M. Facile Assembly of G-C_3N_4/Ag_2CO_3/Graphene Oxide with a Novel Dual Z-Scheme System for Enhanced Photocatalytic Pollutant Degradation. *Appl. Surf. Sci.* **2019**, *475*, 421–434. [CrossRef]
60. Rosman, N.; Salleh, W.N.W.; Mohamed, M.A.; Harun, Z.; Ismail, A.F.; Aziz, F. Constructing a Compact Heterojunction Structure of Ag_2CO_3/Ag_2O in-Situ Intermediate Phase Transformation Decorated on ZnO with Superior Photocatalytic Degradation of Ibuprofen. *Sep. Purif. Technol.* **2020**, *251*, 117391. [CrossRef]
61. Alexopoulou, C.; Petala, A.; Frontistis, Z.; Drivas, C.; Kennou, S.; Kondarides, D.I.; Mantzavinos, D. Copper Phosphide and Persulfate Salt: A Novel Catalytic System for the Degradation of Aqueous Phase Micro-Contaminants. *Appl. Catal. B Environ.* **2019**, *244*, 178–187. [CrossRef]
62. Arvaniti, O.S.; Petala, A.; Zalaora, A.-A.; Mantzavinos, D.; Frontistis, Z. Solar Light-Induced Photocatalytic Degradation of Methylparaben by g-C_3N_4 in Different Water Matrices. *J. Chem. Technol. Biotechnol.* **2020**, *95*, 2811–2821. [CrossRef]
63. Wang, J.; Wang, S. Reactive Species in Advanced Oxidation Processes: Formation, Identification and Reaction Mechanism. *Chem. Eng. J.* **2020**, *401*, 126158. [CrossRef]
64. Wang, J.; Wang, S. Effect of Inorganic Anions on the Performance of Advanced Oxidation Processes for Degradation of Organic Contaminants. *Chem. Eng. J.* **2021**, *411*, 128392. [CrossRef]
65. Kumar, A.; Chandel, M.; Sharma, A.; Thakur, M.; Kumar, A.; Pathania, D.; Singh, L. Robust Visible Light Active PANI/$LaFeO_3$/$CoFe_2O_4$ Ternary Heterojunction for the Photo-Degradation and Mineralization of Pharmaceutical Effluent: Clozapine. *J. Environ. Chem. Eng.* **2021**, *9*, 106159. [CrossRef]
66. Azarpira, H.; Sadani, M.; Abtahi, M.; Vaezi, N.; Rezaei, S.; Atafar, Z.; Mohseni, S.M.; Sarkhosh, M.; Ghaderpoori, M.; Keramati, H.; et al. Photo-Catalytic Degradation of Triclosan with UV/Iodide/ZnO Process: Performance, Kinetic, Degradation Pathway, Energy Consumption and Toxicology. *J. Photochem. Photobiol. A Chem.* **2019**, *371*, 423–432. [CrossRef]
67. Li, J.; Zhou, Q.; Yang, F.; Wu, L.; Li, W.; Ren, R.; Lv, Y. Uniform Flower-like BiOBr/BiOI Prepared by a New Method: Visible-Light Photocatalytic Degradation, Influencing Factors and Degradation Mechanism. *New J. Chem.* **2019**, *43*, 14829–14840. [CrossRef]
68. Ma, W.; Wang, N.; Fan, Y.; Tong, T.; Han, X.; Du, Y. Non-Radical-Dominated Catalytic Degradation of Bisphenol A by ZIF-67 Derived Nitrogen-Doped Carbon Nanotubes Frameworks in the Presence of Peroxymonosulfate. *Chem. Eng. J.* **2018**, *336*, 721–731. [CrossRef]
69. Ma, W.; Wang, N.; Du, Y.; Tong, T.; Zhang, L.; Andrew Lin, K.-Y.; Han, X. One-Step Synthesis of Novel Fe_3C@nitrogen-Doped Carbon Nanotubes/Graphene Nanosheets for Catalytic Degradation of Bisphenol A in the Presence of Peroxymonosulfate. *Chem. Eng. J.* **2019**, *356*, 1022–1031. [CrossRef]
70. Dehghan, S.; Kakavandi, B.; Kalantary, R.R. Heterogeneous Sonocatalytic Degradation of Amoxicillin Using ZnO@Fe_3O_4 Magnetic Nanocomposite: Influential Factors, Reusability and Mechanisms. *J. Mol. Liq.* **2018**, *264*, 98–109. [CrossRef]
71. Qiu, P.; Chen, H.; Jiang, F. Cobalt Modified Mesoporous Graphitic Carbon Nitride with Enhanced Visible-Light Photocatalytic Activity. *RSC Adv.* **2014**, *4*, 39969–39977. [CrossRef]
72. Jiang, J.; Gao, J.; Li, T.; Chen, Y.; Wu, Q.; Xie, T.; Lin, Y.; Dong, S. Visible-Light-Driven Photo-Fenton Reaction with α-Fe_2O_3/BiOI at near Neutral PH: Boosted Photogenerated Charge Separation, Optimum Operating Parameters and Mechanism Insight. *J. Colloid Interface Sci.* **2019**, *554*, 531–543. [CrossRef] [PubMed]
73. Yu, C.; Li, G.; Kumar, S.; Yang, K.; Jin, R. Phase Transformation Synthesis of Novel Ag_2O/Ag_2CO_3 Heterostructures with High Visible Light Efficiency in Photocatalytic Degradation of Pollutants. *Adv. Mater.* **2014**, *26*, 892–898. [CrossRef] [PubMed]